Nano Research

ISSN 1998-0124 CN 11-5974/O4
https://doi.org/10.1007/s12274-019-2453-1

Research Article

Growth of 12-inch uniform monolayer graphene film on molten glass and its application in PbI_2-based photodetector

Zhaolong Chen[1,2], Haina Ci[1,2], Zhenjun Tan[1,2], Zhipeng Dou[3], Xu-dong Chen[1], Bingzhi Liu[1,2], Ruojuan Liu[1,2], Li Lin[1,2], Lingzhi Cui[1,2], Peng Gao[3,4], Hailin Peng[1,2,4], Yanfeng Zhang[4,5] (✉), and Zhongfan Liu[1,2,4] (✉)

[1] *Center for Nanochemistry (CNC), Beijing Science and Engineering Center for Nanocarbons, College of Chemistry and Molecular Engineering, Peking University, Beijing 100871, China*
[2] *Beijing National Laboratory for Molecular Sciences, Beijing 100871, China*
[3] *Electron Microscopy Laboratory, School of Physics, Peking University, Beijing 100871, China*
[4] *Beijing Graphene Insititue (BGI), Beijing 100095, China*
[5] *Department of Materials Science and Engineering, College of Engineering, Peking University, Beijing 100871, China*

Received: 27 April 2019 / **Revised:** 2 June 2019 / **Accepted:** 3 June 2019

ABSTRACT

Direct growth of large area uniform graphene on functional insulating materials is essential for engineering versatile applications of graphene. However, the existing synthesis approaches can hardly avoid the generation of non-uniform multilayer graphene along the gas flow direction, affording huge challenges for further scaling up. Herein, by exploiting the molten state of soda-lime glass, we have accomplished the direct growth of large area uniform (up to 30 cm × 6 cm) graphene via a facile chemical vapor deposition route on low cost soda-lime glass. The use of molten glass eliminates the chemically active sites (surface corrugations, scratches, defects), and improves the mobility of carbon precursors, affording uniform nucleation and growth of monolayer graphene. Intriguingly, thus-obtained graphene acts as an ideal coating layer for the surface crystallographic modification of soda-lime glass, making it epitaxy substrates for synthesizing high-quality PbI_2 nanoplates and continues films. Accordingly, a prototype photodetector was fabricated to present excellent photoelectrical properties of high responsivity (~ 600 on/off current ratio) and fast response speed (18 μs). This work hereby paves ways for the batch production and the direct applications of graphene glass as platforms for constructing high performance electronic and optoelectronic devices.

KEYWORDS

graphene, chemical vapor deposition, dielectric substrate, lead iodide, photodetector

Graphene, a two-dimensional atomic crystal which consists of sp^2-bonded carbon atoms arranged in a hexagonal lattice, has been recognized as a promising material in the applications of field-effect transistors [1], transparent electrodes [2], energy-storage devices [3], etc., due to its superior optical [4], electrical [5] and mechanical properties [6]. However, considering of the atomic thin nature of graphene, a supporting substrate is definitely needed for engineering its versatile applications [7]. Fortunately, glass is one kind of widely used amorphous oxide material having a long-lasting history, and shares many compatible properties with graphene, such as good optical transparency and chemical durability. More significantly, direct synthesis of graphene on glass (herein named graphene glass) can endow glass with brand new properties, i.e., electrical and thermal conductivities, surface hydrophobicity, surface crystallographic modification, thus affording quite new application scenarios for both graphene and glass [7].

Recently, our group have developed several routes for the direct growth of graphene films on glass by a chemical vapor deposition (CVD) method. Among these, high-temperature resistant solid glass (such as quartz and sapphire glass) are customarily used as substrates to grow graphene films with mixture of monolayer, bilayer and few layer [8, 9]. Particularly, soda-lime glass is used as substrate for graphene growth from the viewpoint of dramatically lowering the cost of product [10, 11]. Nevertheless, the achieved graphene glass is still limited to small physical dimensions (less than 2 inches in diagonal size). The huge obstacle is that, in the atmospheric pressure CVD (APCVD) process, the concentration of the active carbon species are gradually increased along the gas flow direction in the heating zone [12]. This leads to non-uniform distribution of the active carbon species and variable graphene thicknesses between upstream and downstream positions of the sample. This nonuniform thickness distribution can be enhanced especially when the glass surface possesses abundant active sites (surface corrugations, scratches, defects) that are much easier for graphene nucleation [13, 14]. Accordingly, a surface self-limited growth mechanism is desirable for growing large area uniform graphene glass.

Various prototype devices (e.g., joule heating devices, touch panels, smart windows) have been constructed by our group based on the transparent and conducting feature of graphene glass [13, 15]. In terms of performance, it is still challenging for graphene glass to surpass ITO glass as transparent electrodes for its relative high sheet resistance, apart from cost [16]. However, the as-grown graphene could serve as a crystalline coating layer for the surface crystallographic modification of glass, assisting the growth of functional films on it, such as aluminum nitride, zinc oxide [17, 18]. Hereby, the graphene glass could serve as a perfect platform for growing functional layers, considering its high compatibility with the conventional synthetic routes like metal organic CVD (MOCVD) and molecular beam

Address correspondence to Zhongfan Liu, zfliu@pku.edu.cn; Yanfeng Zhang, yanfengzhang@pku.edu.cn

epitaxy (MBE) [19].

In this study, we report the development of an economical synthesis route for growing large-area uniform, monolayer graphene on the molten state of soda-lime glass, with the size up to 30 cm × 6 cm (only limited by the size of the CVD chamber). According to our in-depth investigations of the growth processes under optimized precursor feeding rates and growth temperature, a surface self-limited growth process/mechanism is proposed. Moreover, the obtained high-uniformity graphene glass is found to be a perfect platform for the epitaxial growth of lead iodide (PbI_2) nanoplates and films by virtue of the crystal structure of graphene. A kind of prototype photodetector is also fabricated to show extremely low dark current (~ 10^{-11} A), high sensitivity (~ 600 on/off current ratio), and fast response speed (18 μs).

The synthetic approach developed in this work involves the shaping of molten glass in a graphite molding module under hydrogen (H_2) and argon (Ar) carriers flows, and the subsequent growth of graphene by using methane (CH_4) as carbon feedstock at the APCVD condition (Fig. S1 in the Electronic Supplementary Material (ESM)). We use the commercial soda-lime glass as growth substrate, which chemical contents are shown in Fig. S2 in the ESM. With this route, the glass substrate turns into homogeneous liquid state at the growth temperature (e.g., 1,020 °C), since it is far above the softening point of soda-lime glass. At the growth stage, the chemically active sites such as surface scratches or defects associated with the solid state surfaces are greatly eliminated, providing ultra-flat, defect free platforms. After the surface is fully covered with a graphene film, further nucleation is dramatically suppressed, enabling the homogeneous growth of large-area uniform graphene, as similarly reported for graphene growth on the liquid copper surface [20].

To highlight the capability of synthesizing large-area uniform monolayer graphene on molten glass, the largest graphene glass sample (30 cm × 6 cm, with the size only limited by the dimension of the reaction chamber) is achieved under the current growth route. For comparison, the direct synthesis of graphene on quartz glass is also performed under the similar condition (Fig. 1(a)). Nearly a same color contrast can be noticed from left to right parts of the sample (graphene/molten glass), indicating the excellent uniformity of the graphene thickness. However, the graphene grown on quartz glass presents gradually increased color change along the gas flow direction (from left to right, from light grey to intense grey), indicating gradually increased graphene thicknesses. This disparate growth behavior can be explained that, the active carbon species is greatly increased along the gas flow direction in the heating zone, leading to fast growth of multilayer graphene at the downstream location of the solid glass, especially when the glass surface are decorated with lots of active sites (surface corrugations, scratches, defects). In contrast, under the similar precursor feeding condition, the ultra-smooth surface of molten glass and the improved migration speed of carbon species on it can prevent the growth of a second layer on the same nucleus, enabling the evolution of large-area uniform monolayer graphene [20].

To further evaluate the uniformity of synthesized graphene, Raman and UV–Vis measurements are then performed at selected points of the large size graphene glass samples (marked in Fig. 1(a), synthesized on molten glass and quartz glass, respectively). Corresponding transmittance measurement results are also shown in Fig. 1(b). It can be noticed that, the transparency of the graphene/quartz glass sample gradually decreases from left to right, while only negligible variation can be observed on the graphene/molten glass sample. Moreover, the corresponding Raman spectra for graphene/molten glass present the same D band peaks (~ 1,350 cm^{-1}) and 2D band peaks (~ 2,694 cm^{-1}) (Fig. 1(c)), which further confirm the good film uniformity over the lateral distance of 30 cm. However, the shapes of the Raman spectra of graphene films on quartz glass are inconsistent from point to point. And the intensity of 2D peak increases obviously from left to right, indicating the formation of multilayer graphene at the right positions (Fig. 1(d)). Moreover, the AFM image of direct-grown graphene/molten glass reveals continuous and ultra-smooth properties, with a root mean square (RMS) roughness ≈ 0.815 nm (Fig. 1(e) top panel). However, the transferred graphene film on glass with the aid of poly(methyl methacrylate) presents many wrinkles and breakages with a RMS roughness ≈ 1.14 nm, owing to the skill-demanding transfer process (Fig. 1(e) bottom panel) [21]. Those results indicate that, large-area uniform graphene film can be synthesized on molten glass, possibly following

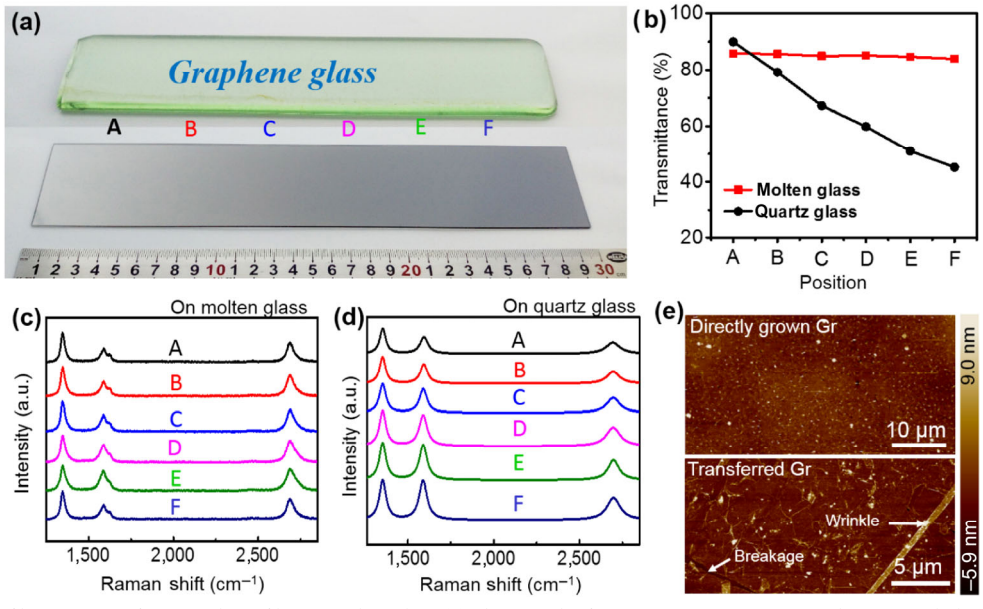

Figure 1 Achievements of large-area uniform graphene film on molten glass. (a) Photograph of as-grown 30 cm × 6 cm graphene on soda-lime glass (up) and on quartz glass (down) under the similar growth condition (1,040 °C, 500 sccm Ar, 50 sccm H_2, 15 sccm CH_4, 4 h, 3-inch tube). (b) Transmittance (at 550 nm) of as-grown graphene films on molten and quartz glass collected from positions labeled A–F in (a) showing different film thickness uniformity, respectively. (c) and (d) Raman spectra of as-grown graphene films on molten (c) and quartz glass (d) collected from positions labeled A–F in (a), respectively. (e) AFM height images of thus obtained graphene glass (top panel) and transferred graphene films on glass (bottom panel), respectively. The CVD-grown graphene on molten glass presents superior surface flatness than that of the transferred graphene on glass which is usually featured with wrinkles and breakages.

a surface self-limited growth mechanism.

To confirm the unique monolayer growth behavior, more systematic experiments are performed by gradually increasing the growth time but with other conditions kept constant. Figure 2(a) shows a photograph of the graphene glass synthesized with increased growth time from 2 to 5 h (with an interval of 1 h). Notably, the molten glass substrates manifest almost no megascopic color change after several hours CVD growth, as demonstrated by their good transparency to the underneath words "Graphene". The existence of highly uniform graphene coating layer on respective samples is further confirmed by SEM images (Figs. 2(b)–2(e)), as well as Raman spectroscopy data (Fig. 2(f)). For the growth time ≈ 2 h, the glass surface is fully covered with graphene, as evidenced by the formation of a uniform thin film over the glass substrate. Particularly, the graphene growth for ≈ 5 h (Fig. 2(e)) yielded a similar structure to that grown for ≈ 2 h. For comparison, graphene films are also grown on solid glass, e.g., fused quartz and sapphire. The graphene thickness variations on fused quartz substrates are clearly observed by the SEM images in Fig. S3 in the ESM, as characterized with gradually increased SEM contrasts (marked with pink and red circles). Notably, the densities of the additional nuclei on the base layer are increased with prolonging growth time, corresponding to the formation of bi- or few layers (Fig. S3 in the ESM). Accordingly, the graphene growth on solid glass should obey a Stranski-Krastanov growth mode rather than a Frank-van der Merwe mode.

Raman spectra of the as-grown samples are also collected to evaluate the thickness variations of as-synthesized graphene on molten glass samples (grown for 2–5 h), as shown in Fig. 2(f). All of them display the characteristic Raman peaks of graphene, showing typical D ≈1,350 cm^{-1}, G ≈1,595 cm^{-1}, 2D ≈ 2,693 cm^{-1} peaks [22]. More significantly, those Raman spectra reveal similar I_{2D}/I_G(> 1.5), highly suggesting the formation of predominant monolayer graphene

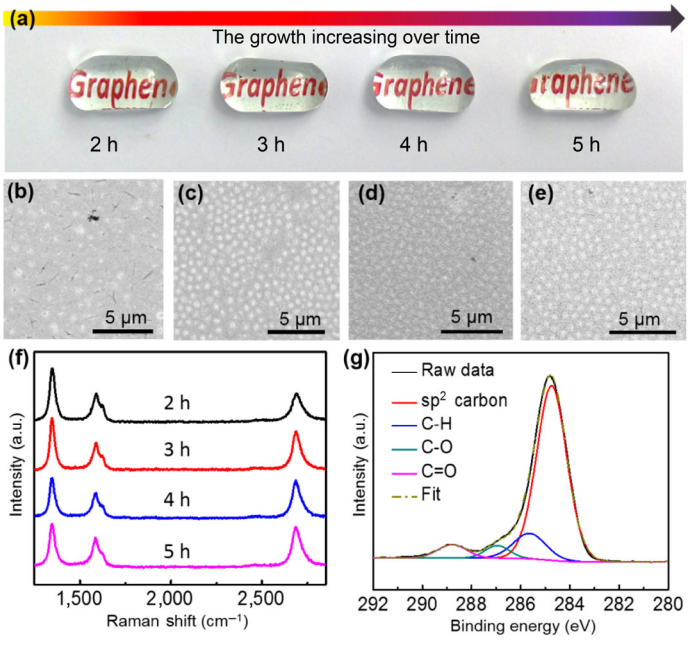

Figure 2 Time-dependent-growth results for graphene growth on molten glass. (a) Photograph of as-grown graphene on molten glass achieved at different growth time of 2, 3, 4, 5 h, respectively, featured with nearly the same transparency. All the other growth parameters are kept identical (~ 1,020 °C, $Ar/H_2/CH_4$: 150/30/15 sccm, 1-inch tube). (b)–(e) Corresponding SEM images of graphene grown on molten glass at various growth time, respectively. (f) Corresponding Raman spectra of graphene grown on molten glass for different growth time from 2–5 h, showing the similar characteristic Raman signal for monolayer graphene. (g) C 1s XPS spectrum of the typical graphene glass hybrid, with the presence of an intense sp^2 carbon peak (284.8 eV), a weak C–H peak (285.6 eV), and two weak peaks of C–O peak (≈ 287.3 eV) and C=O peak (≈ 289.6 eV), respectively.

regardless the growth time extending from 2 to 5 h. In addition, the C 1s X-ray photoelectron spectroscopy (XPS) spectrum (Fig. 2(g)) of graphene glass presents the characteristic signals of graphene with an intense sp^2 carbon peak (284.8 eV), a weak C–H peak (285.6 eV), and weak peaks of C–O peak (~ 287.3 eV) and C=O peak (~ 289.6 eV) [23]. Based on the above results, a surface self- limited growth behavior of graphene on molten glass can be determined with the evolution of large-scale homogenous, monolayer graphene. This growth behavior resembles the growth of graphene on Cu foils under the low-pressure CVD (LPCVD) condition, forming predominantly monolayer graphene under a specific growth conditon [24].

The as-grown graphene on soda-lime glass (grown for 5 h) is further examined with optical microscope (OM), atomic force microscope (AFM) and transmission electron microscopy (TEM) after a sample transfer process. The optical microscope image (Fig. 3(a)) of the transferred graphene on the SiO_2/Si substrate presents well-distributed, uniform pink color contrast all over the surface, indicating its relative high thickness uniformity. Moreover, the AFM height image of the transferred graphene film (Fig. 3(b)) reveals a clear contrast with regard to the SiO_2/Si substrate, showing an invariable thickness of ≈ 0.71 nm at different locations, the same as the published reference for monolayer graphene on SiO_2/Si [25]. Furthermore, the corresponding low magnification TEM image manifests the typical contrast of a continuous graphene film (Fig. S4 in the ESM). The layer number is also identified to be monolayer from the edge of breakage under the high-resolution TEM (HR-TEM) views, as representatively shown in Fig. 3(c). For more proofs, the graphene film is also transferred onto fused quartz for optical transparency characterizations. It exhibits a good transmittance of ~ 97.2% at a wavelength of 550 nm (Fig. 3(d)), again suggesting the monolayer character of our synthesized graphene film on molten glass [26]. Moreover, the graphene samples grown with different growth time (2, 3, 4, 5 h) manifest the similar monolayer characteristic, thus confirming the self-limited growth feature on molten glass.

As known that, the graphene growth on copper foils is highly dependent on the growth condition. For example, at a relative high methane concentration, monolayer, bilayer and even thicker layers coexisted on Cu foils in an APCVD process, which is in contrast with the LPCVD case with the formation of predominantly monolayer graphene [27]. In the current growth system, we find that the graphene growth behavior on molten glass is also influenced by the CVD growth condition. To address this, a series of experiments are performed within the commonly used temperature interval (1,000–1,080 °C) to explore the applicable condition for the large-area uniform monolayer graphene growth, with the results shown in Fig. 3(e). At high flow rates of CH_4 (above the marked area), the concentration of active carbon species is high enough to induce gas phase reactions with the formation of carbon particles in the gas flow. Particles then deposited on the bare molten glass or the predeposited graphene, resulting in multilayer graphene nucleation and growth. At relative low flow rates of CH_4 (under the marked area), the concentrations of active carbon species are too low to meet the requirement for graphene nucleation and growth. In this regard, dominant single-layer graphene is synthesized on molten glass within a narrow parameter range that is determined by the balance of growth temperature and CH_4 flow range, as marked in Fig. 3(e).

Besides, the kinetics (herein, relates to the surface morphological state of substrate) is also proposed to impose important ramifications on the film uniformity across a large area, as well as influence the growth rate of graphene. As shown in the sketch map in Figs. 4(a) and 4(e), scratches or defects on quart glass can serve as nucleation sites, leading to random nucleation and nonuniform growth of graphene. However, this issue can be greatly suppressed on the ultraflat surface of molten glass. To confirm this, a systematic comparison have been made regarding the growth results on molten glass and

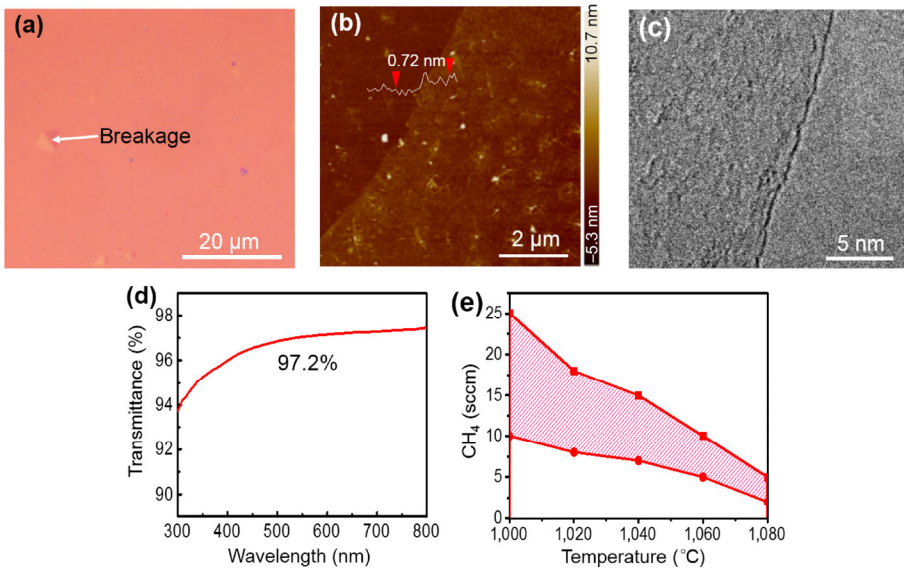

Figure 3 Layer thickness characterizations of graphene synthesized on molten glass. (a) Optical microscope image of the transferred graphene film on the SiO_2/Si substrate showing its large area uniformity (~ 1,020 °C, Ar/H_2/CH_4: 150/30/15 sccm, 5 h, 1-inch tube). (b) Corresponding AFM height image of the transferred graphene film showing a typical layer thickness of ~ 0.72 nm. (c) HR-TEM image on the edge of the graphene film confirming its monolayer feature. (d) Typical UV–Vis spectrum of the transferred graphene film on quartz glass providing further evidence of the monolayer feature (transparency ~ 97.2%). (e) Window for the flow rate of CH_4 under different growth temperature towards the formation of uniform monolayer graphene on molten glass with all the other parameters kept constant (Ar: 150 sccm, H_2: 30 sccm).

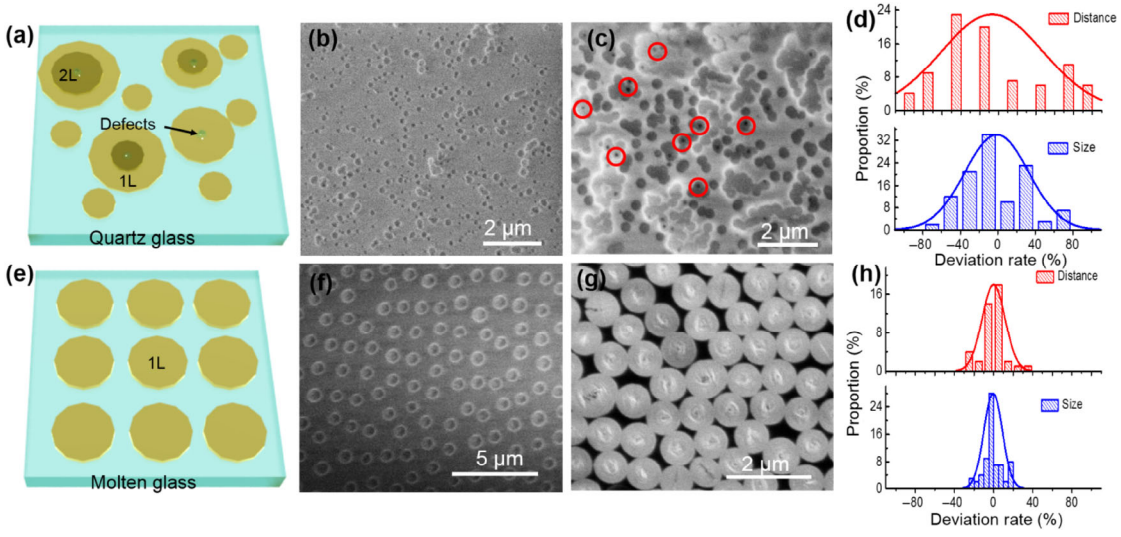

Figure 4 Comparison of the nucleation uniformity and inter-nuclei distance of graphene on molten glass and quartz glass, respectively. (a) and (e) Sketch maps of the nucleation of graphene on quartz glass (a) and molten glass (e), respectively. (b) and (c) SEM images of graphene on quartz glass at the growth time of 40 min (b) and 75 min (c), respectively (1,020 °C, 150 sccm Ar, 30 sccm H_2, 15 sccm CH_4). (d) Statistical distribution about the deviations of size and inter-domain distance of graphene nucleus on quartz glass as shown in (b). (f) and (g) SEM images of graphene on molten glass at the growth time of 40 min (f) and 60 min (g), respectively (1,020 °C, 150 sccm Ar, 30 sccm H_2, 15 sccm CH_4, 1-inch tube). (h) Statistical distributions about the deviation of size and inter-nuclei distance of graphene nucleus on molten glass as shown in (f).

on high-temperature resistant glass substrates (e.g., fused quartz, sapphire) under the similar conditions. In the early stage of graphene growth, nonuniformly and randomly dispersed nuclei appeared on quartz glass (Fig. 4(b)), whereas uniformly dispersed nuclei occurred on the molten glass surface (Fig. 4(f)). The corresponding statistical distributions of size and inter-nuclei distance of graphene nucleation are presented in Figs. 4(d) and 4(h). Notably, the typical values of graphene nucleation on quartz glass are ≈ 130.5 and ≈ 203.5 nm, respectively, showing standard deviations of ≈ 45.1 and ≈ 126.7 nm (with the deviation rates of 34.5% and 62.3%, respectively). However, for the molten glass case, the average values are ≈ 703.5 and ≈ 648.3 nm, with greatly reduced deviation rates to 10.7% and 11.7%, respectively. These sharp differences can be attributed to the dramatic disparity between the surface properties of molten and solid glass. First, the liquid surface of molten glass completely eliminates the active sites that always serve as nucleation sites [14], enabling comparative homogeneous, low-density nucleation and large domain size, compared with that on the solid quartz glass surface. Second, the isotropic and ultra-smooth molten surface contributes relative high diffusion rate of C species on it, favoring fast and uniform growth of graphene. Particularly, the difference of graphene grown on quartz and molten glass are exaggerated more significantly with increasing growth time. The individual graphene domains self-assembled into highly ordered structures on molten glass surfaces (Fig. 4(g)). However, soap bubbles spreading on water like morphology appeared on the quartz glass surface (Fig. 4(c)). The nucleation of second or multilayer graphene can also be observed in this case (the dark grey areas as marked by red circles, in contrast to light grey areas corresponding

to the first layer), indicating the unsatisfactory uniformity of graphene synthesized on solid glass. This is further evidenced by the AFM height image and height profile of graphene nuclei on sapphire (Fig. S5 in the ESM).

In a further step, the thus-obtained graphene glass is applied as a substrate to assist the growth of functional films on it, such as PdI_2 by the physical vapor deposition (PVD) process (Fig. 5(a)). Herein, PdI_2 has the similar hexagonal structure with graphene. Moreover, PbI_2 is a widely used direct band gap semiconductor that has wide application potentials in X-ray, c-ray, optical detectors, and perovskite solar cells fabrications [28–31]. To confirm the superiority of the as-grown graphene glass as epitaxy substrate, we grow PbI_2 nuclei on the uncompletely covered graphene glass. Notably, PbI_2 selectively nucleated on the graphene region (disks) and is scarcely deposited on the surface of bare glass (Fig. S6 in the ESM). Then, the typical SEM image of 2D PbI_2 nanoplates synthesized on the graphene glass substrate is displayed in Fig. S7(a) in the ESM, which presents regular hexagonal or triangular shape morphologies. The corresponding SEM energy dispersive X-ray spectroscopy (EDS) elemental mapping manifests the well dispersed Pb (Fig. S7(b) in the ESM) and I signals (Fig. S7(c) in the ESM), confirming the 2D uniformity of the synthesized products. The AFM result of synthesized PbI_2 plates is also displayed in Fig. 5(b) to show its smooth surface property. With the increase of precursor sublimation temperature continues, PbI_2 films are also obtained on the graphene glass surface (Fig. 5(c)). In contrast, irregular PbI_2 structures are usually preferred on the bare glass surface, which is free of graphene coating, as shown in Fig. 5(d). Further Raman spectrum reveals the typical A_{1g} phonon modes (~ 98 cm^{-1}) of as-grown PbI_2 film on graphene glass, as shown in Fig. S8 in the ESM. Additionally, high resolution X-ray photoelectron spectroscopy (XPS) spectra of I $3d_{5/2}$ ($3d_{3/2}$) and Pb $4f_{7/2}$ ($4f_{5/2}$) are also demonstrated in Fig. 5(e), illustrating the relative high crystal quality of the synthesized PbI_2 film.

The aberration-corrected high-angle annular dark field (HAADF) STEM image in Fig. 5(f) clearly shows the perfect crystal lattice of as-grown PbI_2 films (with FFT pattern shown as inset), indicating its rather high crystal quality. The lattice spacing of PbI_2 along three different directions (with an intersection angle of 60°) are all estimated to be ~ 2.3 Å, which correspond to the values of {100} set of planes. Moreover, the atomistic structure model of the PbI_2 with a viewing direction of [001] is consistent with the STEM and FFT pattern results (Fig. 5(g)). The corresponding EDS images confirm the uniformly dispersed Pb and I elements (Fig. 5(h)). Briefly, high crystal quality PbI_2 films can be directly synthesized on thus-obtained graphene glass.

To investigate the opto-electronic properties of the as-grown PbI_2 film on graphene glass, photodetectors are fabricated by depositing Au electrodes on the PbI_2 films (Fig. 5(i) and Fig. S9 in the ESM). The sensitivity and stability of the as-fabricated photodetector is measured by periodically turning on/off the light with different intensity of white light at a bias of 2 V and white light power of 8 $mW{\cdot}cm^{-2}$ (Fig. 5(j)). It exhibits extremely low dark current (~ 10^{-11} A) on the "OFF" state, high on/off current ratio (~ 600), and excellent stability and reversibility (Fig. 5(j)). Apart from stability and sensitivity, the response time is another important parameter for evaluating the performance of a device, as usually measured by an oscilloscope. The rise and decay time are estimated to be ~ 18 and 50 μs, respectively (Figs. 5(k) and 5(l)). These values are much better than that of the other reported 2D materials, indicating the great application potential of PbI_2/graphene glass hybrids in photodetectors [32, 33].

In summary, we have demonstrated that, the use of molten glass is a particularly effective strategy for directly synthesizing large-area uniform graphene film (30 cm × 6 cm). Unlike the use of solid glass, the molten glass offers a low-defect, highly homogeneous and flat

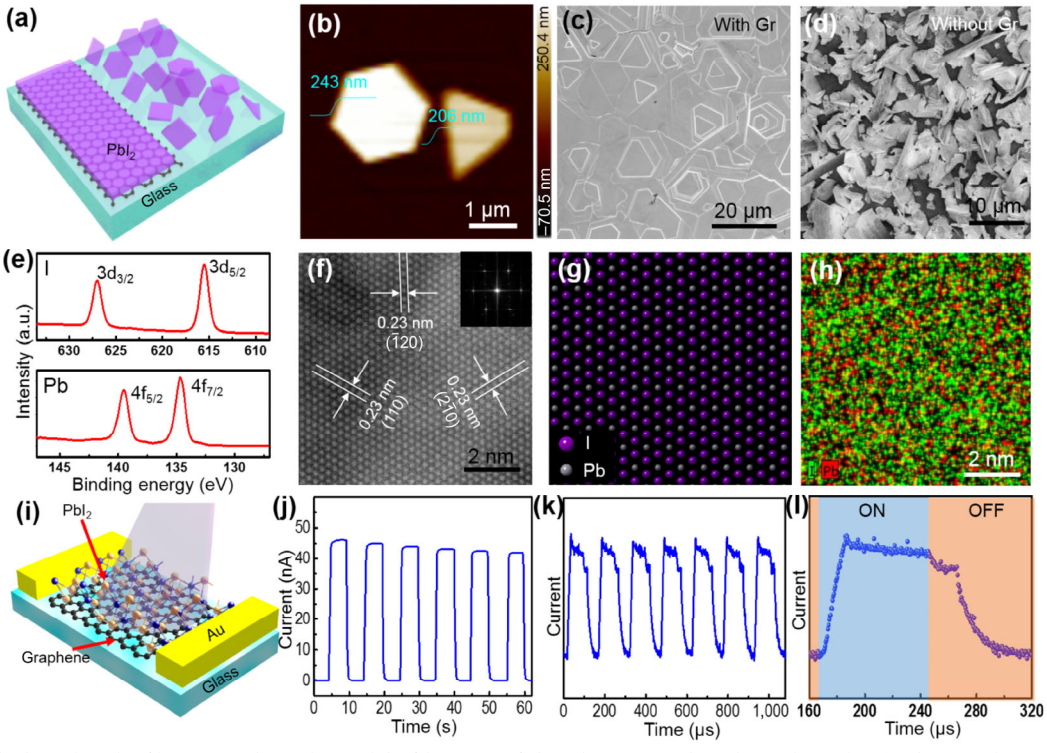

Figure 5 Growth of high-quality PbI_2 films on graphene glass and the fabrication of photodetectors on thus-obtained sample. (a) Schematic diagram of the growth of PbI_2 on glass substrates with and without graphene. (b) AFM image and height profile of synthesized PbI_2 nanoplates on graphene glass. (c) and (d) SEM images of PbI_2 films grown on graphene glass and bare glass under the same growth condition (precursor sublimation temperature ≈ 400 °C, growth time ≈ 0.5 h), respectively. (e) XPS spectrum regarding the binding energies of I 3d and Pb 4f. (f) Atomically resolved HAADF-STEM image of as-grown PbI_2 film and FFT pattern as inset. (g) Corresponding atomistic model structure of the PbI_2 with viewing direction of [001] based on the STEM image and FFT pattern. (h) Corresponding EDS elemental mapping showing the distribution of I (green) and Pb (red). (i) Schematics of the as-fabricated photodetector. (j) Photoresponse of the photodetector device measured at a bias of 2 V and incident power of 8 $mW{\cdot}cm^{-2}$. (k) and (l) Time-dependent photocurrent response of the device operated at a bias voltage of 2 V and an incident power of 100 μW.

template, which induces a relative low nucleation density, fast immigration of carbon species, and growth of predominant monolayer graphene. Thus-obtained large-area uniform graphene film can serve as an ideal coating layer for the surface crystallographic modification of glass. As an example, the graphene glass is served as a perfect platform for the epitaxial growth of high quality PbI_2 nanoplates and films, which is then utilized for constructing high performance opto-electronic devices, featured with a low dark current, high responsivity and fast response speed. In essence, this work provides a reliable pathway for the scalable production of low-cost, highly uniform, monolayer graphene on glass by employing a surface-self-limited growth mechanism, and offers novel insights into the surface crystallographic modification of glass for more versatile applications, especially for the epitaxial growth of functional materials towards constructing high performance opto-electronic devices.

Acknowledgements

The authors acknowledge Electron Microscopy Laboratory in Peking University for the use of Cs corrected electron microscope. This work was financially supported by the National Basic Research Program of China (No. 2016YFA0200103), the National Natural Science Foundation of China (Nos. 51432002 and 51290272), and the Beijing Municipal Science and Technology Planning Project (No. Z161100002116020).

Electronic Supplementary Material: Supplementary material (detailed experimental section, schematic of the growth process, EDX results, SEM images, Raman spectroscopy measurements, TEM image and so on) is available in the online version of this article at https://doi.org/10.1007/s12274-019-2453-1.

References

[1] Meric, I.; Han, M. Y.; Young, A. F.; Ozyilmaz, B.; Kim, P.; Shepard, K. L. Current saturation in zero-bandgap, top-gated graphene field-effect transistors. *Nat. Nanotechnol.* **2008**, *3*, 654–659.

[2] Bae, S.; Kim, H.; Lee, Y.; Xu, X. F.; Park, J. S.; Zheng, Y.; Balakrishnan, J.; Lei, T.; Kim, H. R.; Song, Y. I. et al. Roll-to-roll production of 30-inch graphene films for transparent electrodes. *Nat. Nanotechnol.* **2010**, *5*, 574–578.

[3] Raccichini, R.; Varzi, A.; Passerini, S.; Scrosati, B. The role of graphene for electrochemical energy storage. *Nat. Mater.* **2015**, *14*, 271–279.

[4] Liu, M.; Yin, X. B.; Ulin-Avila, E.; Geng, B. S.; Zentgraf, T.; Ju, L.; Wang, F.; Zhang, X. A graphene-based broadband optical modulator. *Nature* **2011**, *474*, 64–67.

[5] Novoselov, K. S.; Geim, A. K.; Morozov, S. V.; Jiang, D.; Zhang, Y.; Dubonos, S. V.; Grigorieva, I. V.; Firsov, A. A. Electric field effect in atomically thin carbon films. *Science* **2004**, *306*, 666–669.

[6] Lee, C.; Wei, X. D.; Kysar, J. W.; Hone, J. Measurement of the elastic properties and intrinsic strength of monolayer graphene. *Science* **2008**, *321*, 385–388.

[7] Chen, X. D.; Chen, Z. L.; Sun, J. Y.; Zhang, Y. F.; Liu, Z. F. Graphene glass: direct growth of graphene on traditional glasses. *Acta Phys. Chim. Sin.* **2016**, *32*, 14–27.

[8] Sun, J. Y.; Chen, Y. B.; Priydarshi, M. K.; Chen, Z.; Bachmatiuk, A.; Zou, Z. Y.; Chen, Z. L.; Song, X. J.; Gao, Y. F.; Rüemmeli, M. H. et al. Direct chemical vapor deposition-derived graphene glasses targeting wide ranged applications. *Nano Lett.* **2015**, *15*, 5846–5854.

[9] Chen, Z. L.; Guan, B. L.; Chen, X. D.; Zeng, Q.; Lin, L.; Wang, R. Y.; Priydarshi, M. K.; Sun, J. Y.; Zhang, Z. P.; Wei, T. B. et al. Fast and uniform growth of graphene glass using confined-flow chemical vapor deposition and its unique applications. *Nano. Res.* **2016**, *9*, 3048–3055.

[10] Plummer, J. Molten bed. *Nat. Mater.* **2015**, *14*, 1186.

[11] Chen, Y. B.; Sun, J. Y.; Gao, J. F.; Du, F.; Han, Q.; Nie, Y. F.; Chen, Z. L.; Bachmatiuk, A.; Priydarshi, M. K.; Ma, D. L. et al. Growing uniform graphene disks and films on molten glass for heating devices and cell culture. *Adv. Mater.* **2015**, *27*, 7839–7846.

[12] Li, G.; Huang, S. H.; Li, Z. Y. Gas-phase dynamics in graphene growth by chemical vapour deposition. *Phys. Chem. Chem. Phys.* **2015**, *17*, 22832–22836.

[13] Chen, X. D.; Chen, Z. L.; Jiang, W. S.; Zhang, C. H.; Sun, J. Y.; Wang, H. H.; Xin, W.; Lin, L.; Priydarshi, M. K.; Yang, H. et al. Fast growth and broad applications of 25-inch uniform graphene glass. *Adv. Mater.* **2017**, *29*, 1603428.

[14] Han, G. H.; Güneş, F.; Bae, J. J.; Kim, E. S.; Chae, S. J.; Shin, H. J.; Choi, J. Y.; Pribat, D.; Lee, Y. H. Influence of copper morphology in forming nucleation seeds for graphene growth. *Nano Lett.* **2011**, *11*, 4144–4148.

[15] Sun, J. Y.; Chen, Z. L.; Yuan, L.; Chen, Y. B.; Ning, J.; Liu, S. W.; Ma, D. L.; Song, X. J.; Priydarshi, M. K.; Bachmatiuk, A. et al. Direct chemical-vapor-deposition-fabricated, large-scale graphene glass with high carrier mobility and uniformity for touch panel applications. *ACS Nano* **2016**, *10*, 11136–11144.

[16] Novoselov, K. S.; Fal'ko, V. I.; Colombo, L.; Gellert, P. R.; Schwab, M. G.; Kim, K. A roadmap for graphene. *Nature* **2012**, *490*, 192–200.

[17] Shon, J. W.; Ohta, J.; Ueno, K.; Kobayashi, A.; Fujioka, H. Fabrication of full-color InGaN-based light-emitting diodes on amorphous substrates by pulsed sputtering. *Sci. Rep.* **2014**, *4*, 5325.

[18] Chung, K.; Lee, C. H.; Yi, G. C. Transferable GaN layers grown on ZnO-coated graphene layers for optoelectronic devices. *Science* **2010**, *330*, 655–657.

[19] Kumaresan, V.; Largeau, L.; Madouri, A.; Glas, F.; Zhang, H. Z.; Oehler, F.; Cavanna, A.; Babichev, A.; Travers, L.; Gogneau, N. et al. Epitaxy of GaN nanowires on graphene. *Nano Lett.* **2016**, *16*, 4895–4902.

[20] Geng, D.C.; Wu, B.; Guo, Y.L.; Huang, L.P.; Xue, Y.Z.; Chen, J.Y.; Yu, G.; Jiang, L.; Hu, W.P.; Liu, Y.Q. Uniform hexagonal graphene flakes and films grown on liquid copper surface. *Proc. Natl. Acad. Sci. USA* **2012**, *109*, 7992–7996.

[21] Li, X. S.; Zhu, Y. W.; Cai, W. W.; Borysiak, M.; Han, B. Y.; Chen, D.; Piner, R. D.; Colombo, L.; Ruoff, R. S. Transfer of large-area graphene films for high-performance transparent conductive electrodes. *Nano Lett.* 2009, 9, 4359–4363.

[22] Graf, D.; Molitor, F.; Ensslin, K.; Stampfer, C.; Jungen, A.; Hierold, C.; Wirtz, L. Spatially resolved Raman spectroscopy of single- and few-layer graphene. *Nano Lett.* **2007**, *7*, 238–242.

[23] Chen, J. Y.; Wen, Y. G.; Guo, Y. L.; Wu, B.; Huang, L. P.; Xue, Y. Z.; Geng, D. C.; Wang, D.; Yu, G.; Liu, Y. Q. Oxygen-aided synthesis of polycrystalline graphene on silicon dioxide substrates. *J. Am. Chem. Soc.* **2011**, *133*, 17548–17551.

[24] Li, X. S.; Cai, W. W.; An, J.; Kim, S.; Nah, J.; Yang, D. X.; Piner, R.; Velamakanni, A.; Jung, I.; Tutuc, E. et al. Large-area synthesis of high-quality and uniform graphene films on copper foils. *Science* **2009**, *324*, 1312–1314.

[25] Gao, L. B.; Ni, G. X.; Liu, Y. P.; Liu, B.; Castro Neto, A. H.; Loh, K. P. Face-to-face transfer of wafer-scale graphene films. *Nature* **2014**, *505*, 190–194.

[26] Song, H. J.; Son, M.; Park, C.; Lim, H.; Levendorf, M. P.; Tsen, A. W.; Park, J.; Choi, H. C. Large scale metal-free synthesis of graphene on sapphire and transfer-free device fabrication. *Nanoscale* **2012**, *4*, 3050–3054.

[27] Bhaviripudi, S.; Jia, X. T.; Dresselhaus, M. S.; Kong, J. Role of kinetic factors in chemical vapor deposition synthesis of uniform large area graphene using copper catalyst. *Nano Lett.* **2010**, *10*, 4128–4133.

[28] Deng, H.; Yang, X. K.; Dong, D. D.; Li, B.; Yang, D.; Yuan, S. J.; Qiao, K. K.; Cheng, Y. B.; Tang, J.; Song, H. S. Flexible and semitransparent organolead triiodide perovskite network photodetector arrays with high stability. *Nano Lett.* **2015**, *15*, 7963–7969.

[29] Tian, Y. D.; Yan, J. C.; Zhang, Y.; Chen, X.; Guo, Y. N.; Cong, P. P.; Sun, L. L.; Wang, Q. J.; Guo, E. Q.; Wei, X. C. et al. Stimulated emission at 288 nm from silicon-doped AlGaN-based multiple-quantum-well laser. *Opt. Express* **2015**, *23*, 11334–11340.

[30] Zheng, W.; Zhang, Z. J.; Lin, R. C.; Xu, K.; He, J.; Huang, F. High-crystalline 2D layered PbI_2 with ultrasmooth surface: Liquid-phase synthesis and application of high-speed photon detection. *Adv. Electron. Mater.* **2016**, *2*, 1600291.

[31] Roth, S.; Willig, W. R. Lead iodide nuclear particle detectors. *Appl. Phys. Lett.* **1971**, *18*, 328–330.

[32] Lei, S. D.; Wen, F. F.; Ge, L. H.; Najmaei, S.; George, A.; Gong, Y. J.; Gao, W. L.; Jin, Z. H.; Li, B.; Lou, J. et al. An atomically layered InSe avalanche photodetector. *Nano Lett.* **2015**, *15*, 3048–3055.

[33] Yang, S. X.; Li, Y.; Wang, X. Z.; Huo, N. J.; Xia, J. B.; Li, S. S.; Li, J. B. High performance few-layer GaS photodetector and its unique photo-response in different gas environments. *Nanoscale* **2014**, *6*, 2582–2587.